AIAA 2003-3411

Advances In Pneumatic-Controlled High-Lift Systems Through Pulsed Blowing

Gregory S. Jones*
Flow Physics and Control Branch
NASA Langley Research Center, Hampton, VA 23681

Robert J. Englar**
Aerospace, Transportation and Advanced Systems Lab
Georgia Tech Research Institute (GTRI), Atlanta GA 30332

ABSTRACT

Circulation Control technologies have been around for 65 years, and have been successfully demonstrated in laboratories and flight vehicles alike, yet there are few production aircraft flying today that implement these advances. Circulation Control techniques may have been overlooked due to perceived unfavorable trade offs of mass flow, pitching moment, cruise drag, noise, etc. Improvements in certain aspects of Circulation Control technology are the focus of this paper. This report will describe airfoil and blown high lift concepts that also address cruise drag reduction and reductions in mass flow through the use of pulsed pneumatic blowing on a Coanda surface. Pulsed concepts demonstrate significant reductions in mass flow requirements for Circulation Control, as well as cruise drag concepts that equal or exceed conventional airfoil systems.

Symbols

A	Area (ft^2)
b	Span (inches)
C_L	Lift Coefficient
C_D	Drag Coefficient
C_M	Pitching Moment Coefficient
C_μ	Momentum Coefficient
C	Chord (inches)
CCW	Circulation Control Wing
D	Drag (lbs)
DC	Duty Cycle (Time On/ Time Off)
h	Slot height (inches)
LE	Leading Edge
L	Lift (lbs)
M	Pitching Moment (ft-lbs)
$\dot{m}$	mass flow (slug/sec)
P	Pressure (lb/in^2 or lb/ft^2)
p'	Fluctuating Pressure (lb/in^2 or lb/ft^2)
r	Trailing edge radius (inches)
U	Velocity (ft/sec)
u'	Fluctuating Velocity (ft/sec)
q	Dynamic Pressure (lb/ft^2)
S	Wing plan form area (ft^2)
SCFM	Standard Volume Flow (ft^3/min) (Expanded to 14.7 psia & 68°F)
TE	Trailing Edge
T	Static Temperature (°R)
w	Slot Width (inches)
α	Angle of attack (degrees)
ρ	density ($slugs/ft^3$)
Γ	Circulation

Subscripts:

∞	Free stream Conditions
J	Jet at slot exit
o	Stagnation Condition
BAL	Measurements w/ strain gage balance
EQUIV	Equivalent (referenced to drag)

* SENIOR RESEARCH ENGINEER, AIAA SENIOR MEMBER
** PRINCIPAL RESEARCH ENGINEER, AIAA ASSOCIATE FELLOW

INTRODUCTION

Pneumatic control of aerodynamic high lift configurations has been studied for more than 65 years[1, 2]. Wind tunnel, computational, and flight experiments have shown significant benefits of pneumatically controlling the flow field using steady tangential blowing over the rounded Coanda trailing edge of a wing[3, 4, 5]. In spite of the benefits, these techniques have not frequently been applied to production aircraft. Many of the roadblocks have been associated with the engine bleed requirements and cruise penalties associated with blunt blown trailing edges. The desire to use a larger radius Coanda surface for maximum lift is often a tradeoff with a smaller radius Coanda surface for minimum cruise drag [6, 7] as shown in Figure 1.

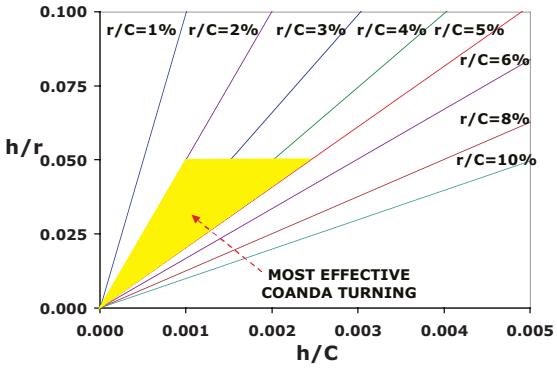

Figure 1 Effective Coanda performance for different radius and jet slot heights[8]

This paper will focus on two airfoil configurations that address these issues through the use of pulsed or unsteady pneumatics. Preliminary research has been accomplished under a NASA-Langley-sponsored program at Georgia Tech Research Institute (GTRI) and NASA LaRC Flow Physics and Control Branch (FPCB). This cooperative investigation focused on pulsed pneumatic technology that is intended to dramatically reduce the mass flow requirements and cruise drag associated with Circulation Control Wings (CCW). These mass flow characteristics are typically described through the momentum coefficient:

$$C\mu = \frac{\dot{m}}{q}\frac{U_J}{CS} \qquad \text{(Eq. 1)}$$

While applications of this technology can be extended to many aircraft configurations, this study was directed towards General Aviation (GA) and Personal Air Vehicles (PAVE).

BASIC AIRFOILS of INTEREST

Two separate 2-D airfoil designs were initiated for possible general aviation use[9] that targeted sectional lift coefficients of 3 and cruise drag coefficients consistent with traditional airfoils. These airfoils, shown in Figures 2 and 3, were both based on 17% supercritical-type airfoil sections with large leading-edge radii to minimize leading edge stall. The NASA airfoil configuration[10] was based on a modified GAW(1) design having dual-slot blowing on a small trailing-edge-radius Coanda surface. The dual-slot blowing is intended to create a virtual trailing edge that minimizes cruise drag but maintains an effective Coanda surface to sustain more than 180° of CC jet turning for high-lift operations.[11]

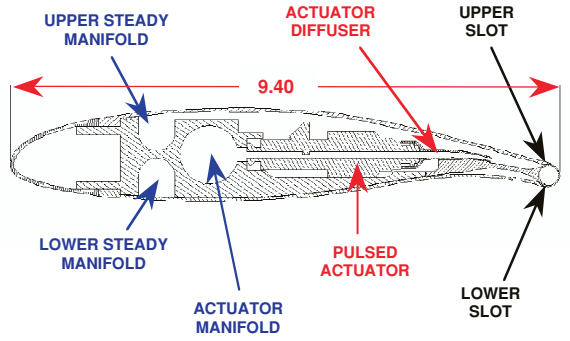

Figure 2. NASA LaRC 2-Dimensional 17% Supercritical General Aviation Circulation Controlled Airfoil (GACC) with a circular trailing edge, r/C = 2%

The GTRI configuration[12] shown in Figure 3 utilized a dual radius CCW trailing edge that capitalizes on a second larger-radius Coanda surface. The small-chord CCW flap shown here is deflected to 90° and can yield up to 135° of CC jet turning for high lift operation. To optimize for cruise conditions the flap can be retracted to create a sharp trailing edge for low cruise drag.

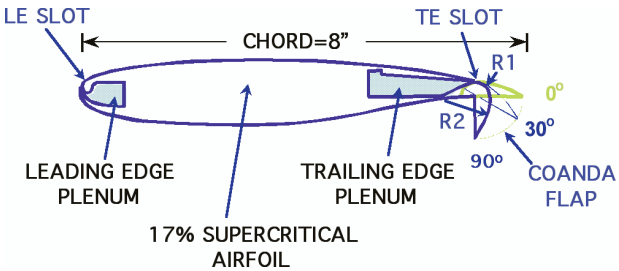

Figure 3. GTRI Dual-Radius CCW with Simple Deflecting Coanda Flap, r_1/C=3.1% r_2/C=15.6%.

Each design has advantages and disadvantages when compared for use in aircraft design, however this study is intended to capture the technologies associated

with basic GA-type wings, where unsteady pneumatic performance is used to reduce required blowing mass flow. Comparisons of these two designs will be made to highlight the physics of the pulsed pneumatic flow control. Both designs were tested with steady and pulsed blowing to capture the change in performance using pulsed jet flow.

Traditionally Circulation Control Wings (CCW) employ a pneumatic modification of the flow field by use of the Coanda effect[3,13]. Figure 4 shows a CFD simulation[11] that highlights streamline turning that are characteristic of CCW techniques. Nominally the streamline turning can be related to lift performance through the augmentation of the circulation around the airfoil that is driven by the Coanda jet at the trailing edge describe by the

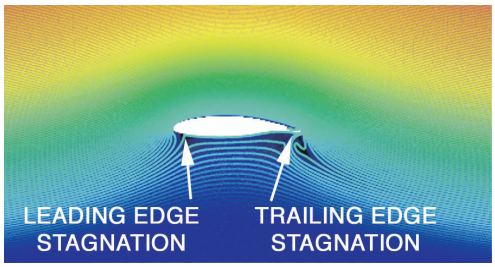

Figure 4 CFD simulation of streamline turning

following CFD simulation. The wall-bounded jet flows along the curved surface and mixes with and acquires the nature of a boundary layer near the wall but becomes that of a free jet at a larger distance from the wall.[14] The degree of jet turning can be related to separation from the surface and can be correlated to the slot height, surface radius, jet velocity, and the Coanda surface geometry shown in Figure 5. Once the jet separates from the Coanda surface it penetrates the low momentum flow from the under surface, creating a pneumatic or virtual flap. Also see References 3, 13 and 14.

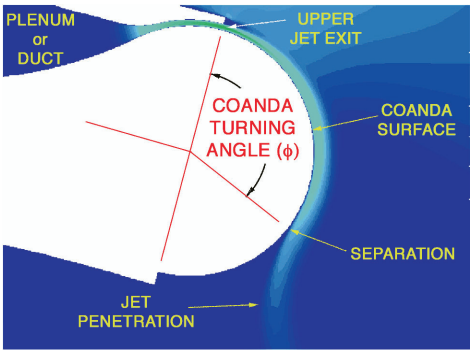

Figure 5 Example of the Coanda effect on a CCW Airfoil.

It is important to recognize that the flow control related to the Coanda effect is often discussed in terms of separation-prevention (boundary–layer control) and super-circulation effects (streamline deflection caused by jet entrainment). One will see in the following discussion, as the boundary layer separation moves around the Coanda surface, the jet momentum simultaneously increases and begins to penetrate and entrain the trailing edge flow field causing the stagnating streamline to change.

At low blowing levels, the jet entrains the outer-flow resulting in the boundary layer attaching to the Coanda surface thus turning the local streamlines, Figure 6(a). As the blowing level is increased, the attachment or separation point moves around the Coanda surface toward the maximum x/C of the airfoil, i.e. x/C=1 shown in Figure 6(b). This will result in the higher momentum jet entraining with the oncoming low momentum flow that emanates from the under-surface flow field. The onset of this jet penetration begins to form a virtual or pneumatic flap that continues to turn the streamlines. The more one blows, the more jet penetration and entrainment occurs, resulting in greater streamline turning.

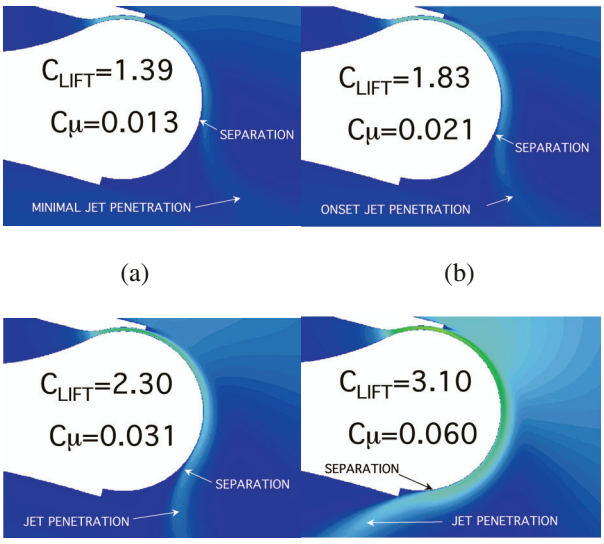

Figure 6 CFD simulation of trailing edge boundary layer control and jet entrainment/penetration around a Coanda surface.

To differentiate between a Coanda flap and other trailing edge control devices, (e.g. conventional flap, jet flap, upper surface blowing, etc.) the flow field is characterized by the variable jet entrainment angle[15] of the Coanda jet compared to that of a fixed jet penetration angle of other devices. This jet entrainment is characteristic of Coanda flows and can cause the

streamlines to deflect beyond potential flow. This unique characteristic is highlighted when the flow is turned beyond the maximum x/C of the airfoil and creates a jet entrainment angle greater than 90° as shown in Figure 6(c). This also gives rise to an increase in suction pressure on the lower Coanda surface and reduces the lift efficiency rate of the Coanda surface. The relationship of reduced lift efficiency and Coanda turning angle is characterized as super-circulation. Further increases in blowing results in jet turning upstream along the lower Coanda surface until a separation limit is reached as shown in Figure 6(d). For the GACC airfoil this separation limit was fixed by the lower surface jet exit that appeared as a forward facing step to the oncoming jet.

For the Dual-radius CC airfoil this angle is determined by the tangent line of the upper surface of the flap at the trailing edge. Once the separation is fixed (approximately 165° for the GACC airfoil and 135° for the Dual radius airfoil) the penetration into the trailing edge flow field is governed by the magnitude of the jet momentum. As the momentum continues to increase, the penetration depth (length) will continue to increase, resulting in increased streamline turning and increased circulation. This increased circulation results in the leading edge stagnation point moving aft along the lower surface resulting in an increase in the leading edge suction pressure. This CC performance is dependant on the jet velocity ratio (blowing pressure), the Coanda surface geometry, jet exit geometry, and the airfoil leading-edge geometries.

EXPERIMENTAL RESULTS

Baseline - Steady Blowing

Subsonic testing of these 2-D blown airfoils were conducted in both the steady state and the pulsed modes in both the NASA Basic Aerodynamic Research Tunnel[16] (BART) and the GTRI Model Test Facility (MTF) research wind tunnels. These tests were performed at Mach numbers less than 0.1 and Reynolds Numbers of approximately 500,000.

NASA BART Steady Tests:

Figure 7 shows the NASA airfoil installed in the BART facility. The GACC model has three modes of operation, *high lift* (upper Coanda blowing), *cruise optimization* (upper and lower blowing on the Coanda surface – dual blowing), and *mass flow optimization* (pulsed upper Coanda blowing). The model was fitted with three interchangeable trailing edges; circular, elliptical, and biconvex. This paper will focus on the circular trailing edge

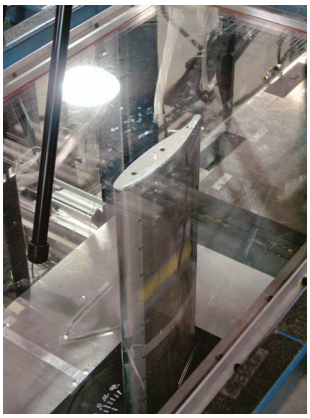

Figure 7- Photo of NASA 2-D GACC airfoil in the BART Tunnel with full span blowing and variable h/C

High Lift Mode

The resultant lift performance characteristics of the GACC airfoil highlight the distinction between separation control and the super-circulation as shown in Figure 8. Whereas greater lift augmentation occurs in the BLC region, high-lift generation continues in the Super-Circulation region but at a lower rate.

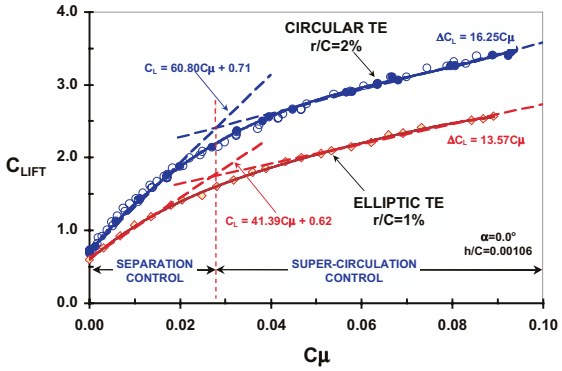

Figure 8- CCW Lift augmentation through separation and super-circulation flow control for GACC airfoil

The GACC experimental lift results evaluated at an angle of attack of zero degrees provide values of lift augmentation $\Delta C_L/C\mu=60$ for the circular trailing edge. The elliptic trailing edge had a lift augmentation of $\Delta C_L/C\mu=41$. This reduction is thought to be related to the trailing edge radius being reduced from 2% to 1% and is consistent with other small-trailing-edge CCW airfoil experiments[3, 12]. It is also noted that both trailing edges break from separation control to super-circulation at the approximate same blowing rate.

The GACC test matrix was limited to lift coefficients of approximately 3 (i.e., no higher blowing was applied). This was consistent with general aviation requirements[17] and wall interference limitations of the GACC model in the NASA BART. The baseline

steady-blowing performance of the 2-D NASA GACC model is characterized by the lift augmentation shown in Figure 9. The high lift characteristics for this CC airfoil are highlighted for both upper and lower blowing.

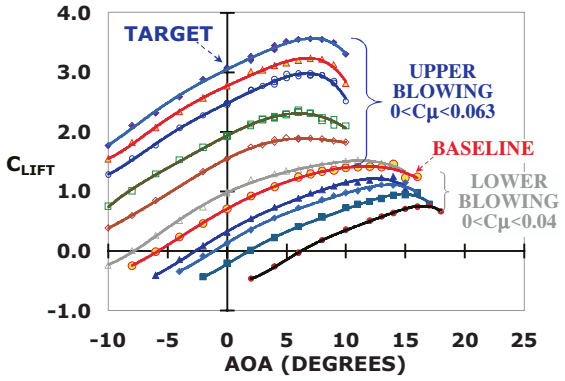

Figure 9- Lift characteristics of the 2-D GACC airfoil using steady blowing (5-component Balance results), r/C=2%, h/r=0.0533, h/C=0.00106

The pressure distribution on the GACC model is shown in figure 10. The large blunt leading edge radius of the GACC model benefits the CC application by minimizing the leading edge separation and distributing the load over a large area of the leading edge.

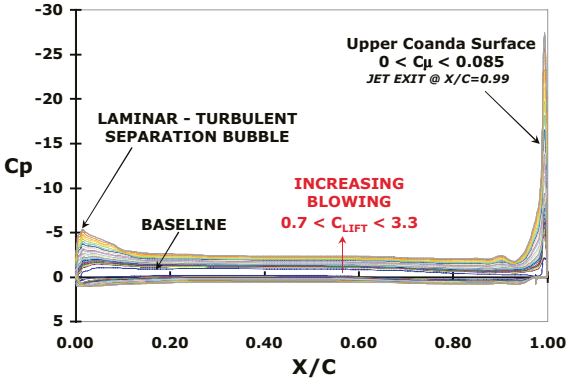

Figure 10 Pressure characteristics of the GACC airfoil, steady blowing at AOA=0°, h/r=0.0533, h/C=0.00106

Careful examination of the leading edge pressure distribution revealed a laminar-turbulent separation bubble. This is thought to be due to the low Reynolds number of this experiment. Initial attempts to eliminate this bubble with boundary layer transition strips were abandoned as the effectiveness of the strips were dependant on the effective angle of attack and leading edge stagnation point.

As steady blowing is applied, both the leading and trailing edge suction pressures increase. The balance of these pressures is reflected in the pitching moment as shown in figure 11. The nose up pitching moment (referenced about 50% chord) peaked near the breakpoint of super-circulation, see figure 8.

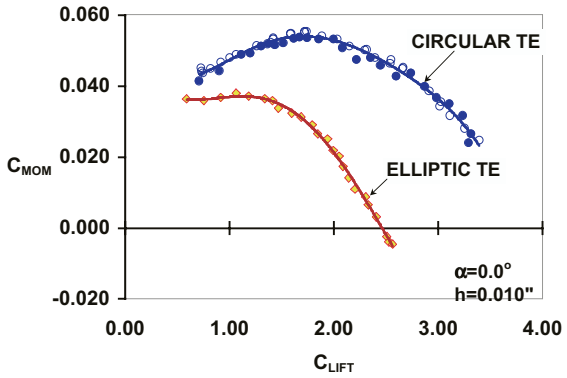

Figure 11 Pitching moment characteristics of the GACC airfoil at zero degrees AOA (Referenced to 50% chord)

The GACC airfoil has a large pressure gradient that is carried over the small Coanda surface. The influence of this pressure on lift, drag, and pitching moment is best reflected in a radial type plot of the trailing edge, where the Coanda surface is unwrapped. The upper surface jet exit is at 0° and the lower jet exit is at 180° as shown in figure 12.

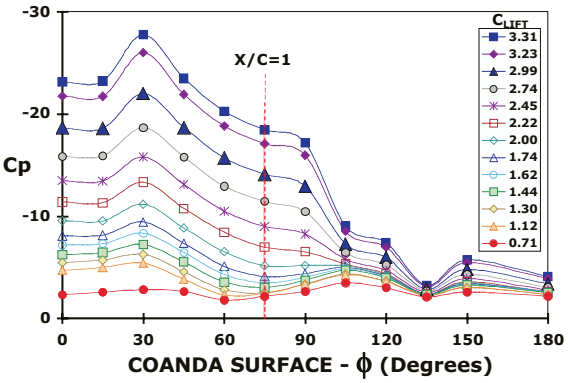

Figure 12 Expansion of circular Coanda trailing edge pressure characteristics for GACC airfoil, Upper Jet exit is located at ϕ=0°(see Figure 5), r/C=2%, AOA=0°

Cruise optimization mode

To minimize the drag for the GACC airfoil simultaneous blowing from the upper and lower jets at the Coanda surface was implemented. To be able to compare CC airfoils with conventional airfoils it is necessary to account for the energy of the airfoil system through an equivalent drag[11,18] This equivalent drag as defined in Reference 11 accounts for momentum and ram drag penalties typically associated with bleed air from an engine. The equivalent cruise drag characteristics for the GACC airfoil in the dual blowing mode are shown in Figure 13. This is consistent with

traditional undeflected flapped airfoils at cruise conditions.

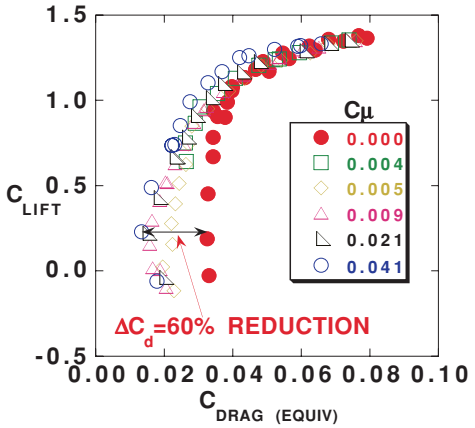

Figure 13 Equivalent Drag polar for 2-D GACC airfoil using dual blowing. Upper and Lower Cμ's are matched.

The upper and lower Cμ were matched in an attempt to rapidly close the wake created by the Coanda surface. The ability to match the conditions of the upper and lower jets was not trivial as the conditions occasionally became unstable. The jet velocity ratios of these cruise conditions were 0.25 to 2.5 of the free stream.

While an equivalent drag is being shown in figure 13, an actual thrust force is being generated. The cruise lift for a representative GA type aircraft would typically be on the order of 0.5. To achieve this with the dual blown CC trailing edge, it is necessary to use an unbalanced upper and lower blowing scheme as shown in figure 14. This method of vectoring the thrust is limited to low values of Cμ for CC applications, as the conditions in small jet exits are being limited to subsonic values to avoid noise issues.

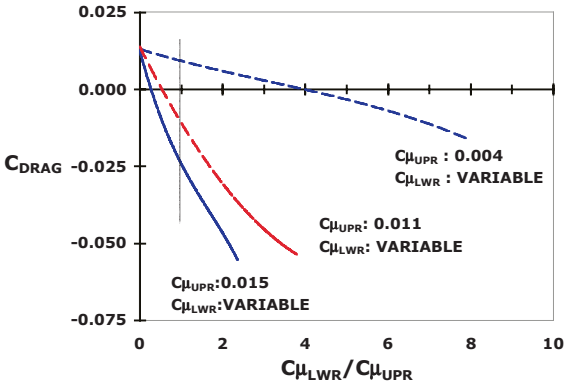

(a) Influenced of unbalanced upper and lower blowing on drag

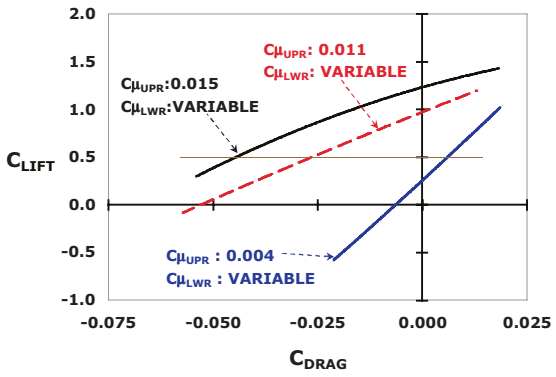

(b) Airfoil cruise performance

Figure 14 Cruise efficiency of dual blown GACC airfoil using unbalanced upper and lower velocity ratios.

GTRI MTF Steady Tests: The steady pneumatic performance of the GTRI Dual-Radius CCW/Supercritical airfoil[12] is similar to the GACC airfoil. The installed leading-edge flow control (tangentially blown LE) dramatically extends the performance of the Dual-Radius CCW airfoil by managing the leading edge separation, as shown in Figure 15. At trailing edge blowing of Cμ=0.15, this LE treatment extends the stall angle from α=-5° to +25°, and C_{lmax} from 5.2 to 6.8.

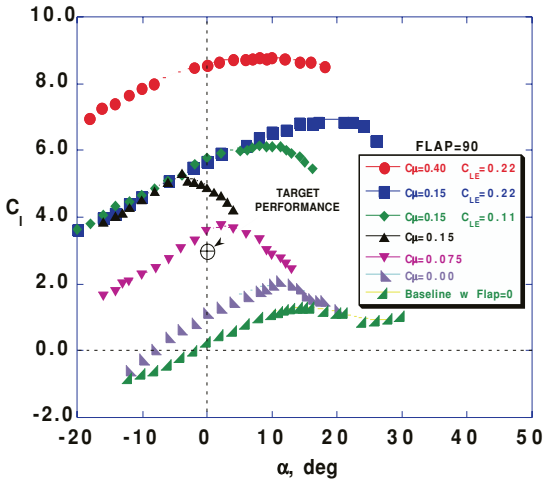

Figure 15 GTRI CCW/Supercritical airfoil, Dual-Radius CCW, R1=0.25", Flap= 90°, Blown L.E.

An added benefit of this single-slotted deflecting-curved-flap CCW configurations is shown in Figures 16 and 17, without leading-edge blowing and all curves at α=0°. Note high lift up to C_L=5.5 at zero incidence generated by TE blowing only, or C_L=7,5 with LE blowing. Also note that these drag polars are produced at α=0° merely by variation in blowing at constant flap angle. The clean baseline airfoil drag polar (which is

produced by αvariation) is shown for comparison, where increase in incidence and high lift always produce greater drag coefficient. With CCW, drag increase or decrease can be produced by varying Cμ only, depending on the flap angle chosen. These benefits are quite promising, but there is still the need to consider the blowing power being expended,

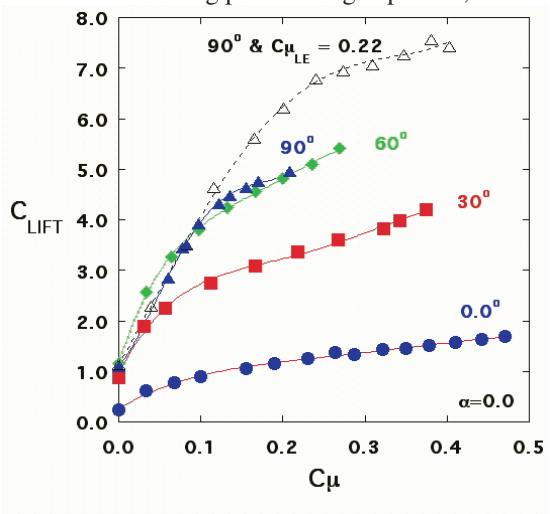

Figure 16- Lift Variation with Blowing and Flap Angle for the CCW Dual-Radius Airfoil, α=0°, h/C=0.0017, No LE Blowing except where noted.

and thus the desire to reduce that requirement by wing pulsed blowing.

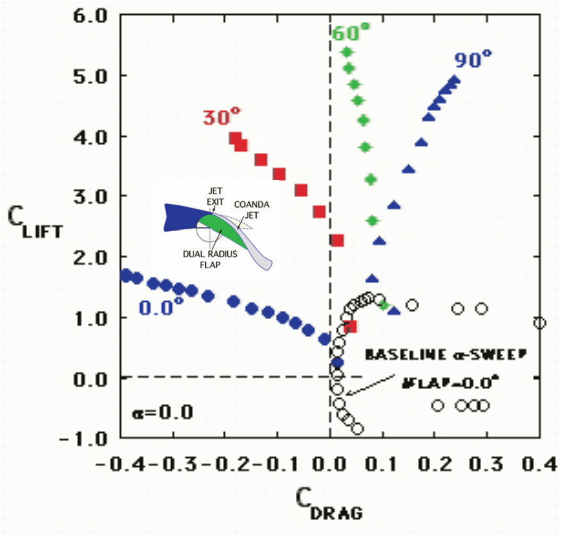

Figure 17- Drag Polars with Blowing and Flap Angle for the CCW Dual-Radius Airfoil, α=0°, h/C=0.0017, No LE Blowing

Pulsed Blowing

This paper will describe two independent pulsed blowing test programs that are based on the airfoils described above. These experiments were conducted on these two blown airfoils to evaluate the gains to be obtained from pulsed blowing. Oyler and Palmer laid the groundwork with pulsed testing of a flat upper surface blown flap described in Ref. 19. They verified that a given C_L could be obtained at lower time-averaged mass flow rates than steady-state values under certain conditions; this was attributed to "increased mixing rate and greater jet velocity produced for a given mass flow. Also, the inertia of the entranced flow requires a time span for the flow to react, resulting in essentially continuous entrainment even between pulses.[20] This further builds on the fact that, for steady state blowing, higher jet velocity ratios from smaller slots at constant Cμ produce better entrainment and lift augmentation, (Refs. 3 and 11).

NASA BART Pulsed Tests: The effectiveness of pulsed blowing on the performance of both of the above airfoil systems is dependent on the efficiency of the pulsing actuator system. This system must include the actuator performance, internal diffuser performance, and the response of the internal volume prior to the jet exit as well as the external time-dependent Coanda effectiveness. Figure 18 shows the NASA airfoil with one of it's uppers skins removed to expose the distributed blowing system.

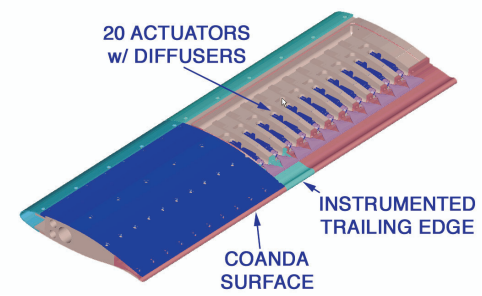

Figure 18 NASA GACC model highlighting the pulsed blowing system located near the jet exit.

The time dependent Coanda response is defined by the unsteady jet profile at the slot exit. Ideally this would be a perfect square wave response at the jet exit. The reality of a perfect square wave diminishes with the complexities of the actuator system, as well as the volume of the plenum and the interaction with the jet slot.

The response of the state-of-the-art high-speed actuator systems used in each of these studies did not generate a perfect-pulsed[21] waveform. The NASA GACC model attempted to minimize the internal volume of the pulsed delivery system by placing the actuators as close to the jet exit as possible. The actuators consisted of 20 high-speed valves that could independently vary duty cycle

(20<DC(%)<80) and frequency (0<Hz<300). Changing the common inlet manifold pressure to the actuators independently varied the time averaged mass flow. Each actuator was operated with pressure ratios that created a sonic condition at the actuator orifice. It was necessary to reshape the velocity profile from a circular jet to a flat uniform distribution at the jet exit via a rapid diffuser. Transmitting the pulse through the diffusers and into the nozzle exit distorts the waveform as shown in an example with thin film data located at the nozzle exit of the GACC airfoil. For the low frequency pulsed jet, the effect of duty cycle is shown in Figure 19

The peak amplitude for the low duty cycle conditions (20% and 30%) does not reach the maximum output performance of the actuator system. The actuator valve being closed before the plenum and actuator volumes have had time to be fully pressurized causes this result. Once the valve is given a "close" command the plenum remains pressurized and continues to bleed air through the jet exit until the plenum pressure reaches ambient conditions.

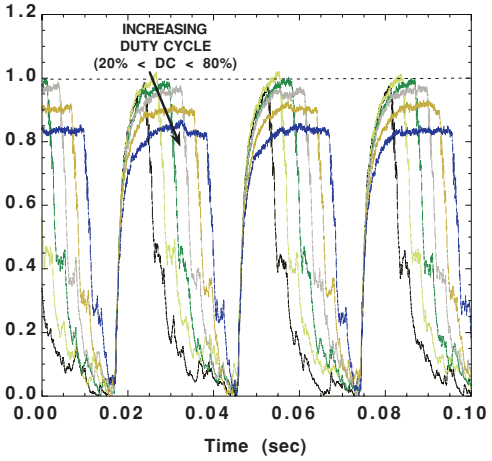

Figure 19 Normalized thin film time history for pulsed CCW at the slot exit. (h= 0.020" and Driver Frequency= 35 Hz)

The actuator system exits into a small plenum then is channeled to the jet exit thru a smooth 10:1 contraction. The jet exits onto the Coanda surface tangentially to the upstream flow. The distortions in the pulsed flow at the jet exit shown in figure 19 are a combination of the actuator distortions and the distortions related to the internal volume between the actuator exit and the jet exit. This process limits the mass flow to the jet exit as indicated by an overall reduction in the peak velocity. In spite of the limitations of the actuator system, the peak velocities do approach sonic conditions. As the drive frequency is increased the actuator efficiency degrades.

To optimize a drive frequency it is desired to know if the flow has any length characteristics that can be capitalized on. Figure 20(a) illustrates the baseline spectra of the GACC airfoil at AOA=0°. There appears a dominant peak at

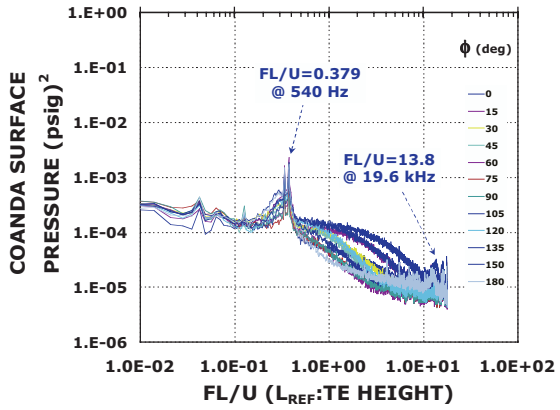

(a) No Blowing - Baseline

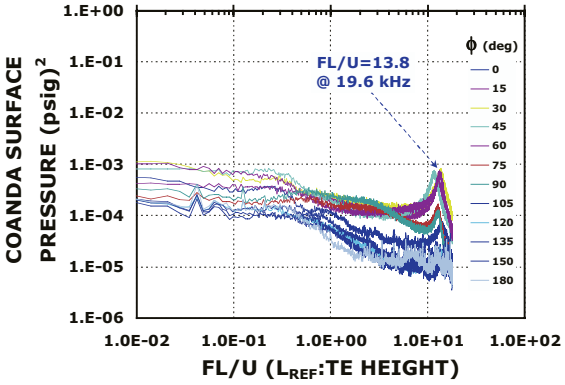

(b) Steady Blowing Cμ=0.007

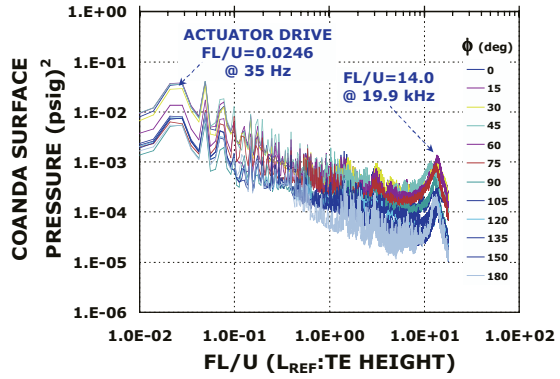

(c) Pulsed Blowing Cμ=0.004, DC=40%

Figure 20 non-dimensional power spectra for GACC circular trailing edge, 100 ensembles, Hanning window

a non-dimensional frequency of approximately 0.38 (540 Hz). This is consistent with audible tones created

by the internal Helmholtz resonance of the blowing system. It is not clear if these tones excited any vortex shedding. There also appears to be an indication of small-scale structures at non-dimensional frequencies of order 14 (19.9kHz). As steady blowing is turned on the audible tone disappeared and the small-scale structure was amplified as shown if Figure 20(b). As blowing levels are increased the effective length of the trailing edge grows due to jet penetration. It is not clear as to the extent of this influence on vortex shedding. Since the small-scale structure at non-dimensional frequencies of order 14 are outside the range of the GACC actuator system, it was determined to operate the pulsed system from 20 to 200 Hz with an emphasis on 35 Hz, Figure 20(c).

Comparing the pressure distribution for pulsed and steady blowing at a lift coefficient of 1.2 is shown in figure 21. These time-averaged pressure magnitudes compare favorably with the pulsed mass flow being 45% less than the steady blowing condition. The phase relationship of the time dependent pressure perturbation along the Coanda surface was used to identify separation. The time-averaged separation point was determined to be between 75° and 90° for this condition.

Comparing the pulsed and steady lift performance of the GACC airfoil for low lift coefficients is shown in Figure 22. A distinct reduction in flow rate due to pulsing can be seen. For a given lift coefficient of 1.0, a 48% reduction in mass flow is realized for a 20% duty cycle when compared to steady blowing. As the duty cycle is increased, the performance benefit decreases. Comparing the lift performance of the pulsed and steady CCW at a fixed average mass flow of 25 SCFM results in the lift coefficient increasing from 0.72 to 1.0 or a 35% lift improvement.

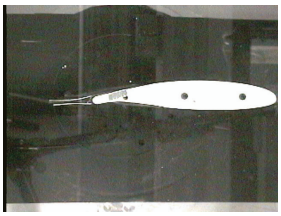

No Blowing

Steady Upper-Blowing

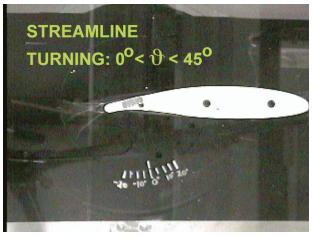

Pulsed Blowing

(a) Streamline turning shown in photo of tufts corresponding to part b & c

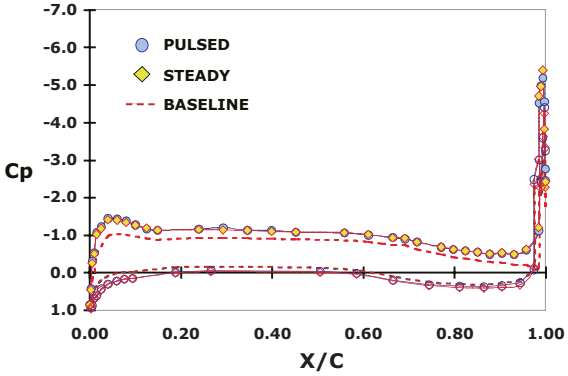

(b) GACC time averaged pressure distribution

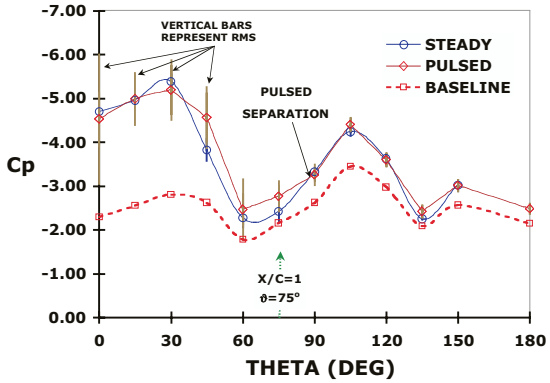

(c) Expansion of trailing edge Cp vs. Coanda angle

Figure 21 Comparison of Pressure characteristics for pulsed and steady blowing of a circular Coanda surface r/C=2%, AOA=0°, pulsed frequency=35 Hz at DC=40%

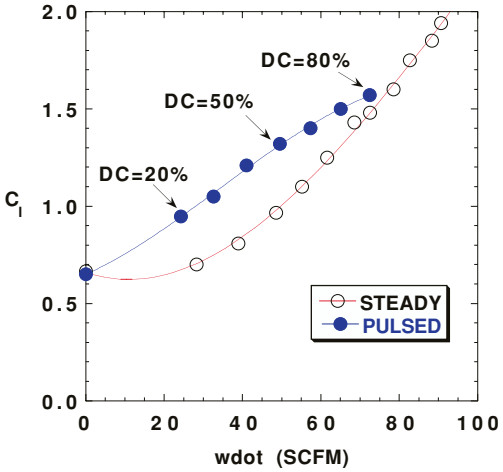

Figure 22- Comparison of pulsed and steady pneumatic control for the GACC airfoil, (Frequency 35 Hz and varying Duty Cycle).

GTRI MTF Pulsed Tests: GTRI personnel conducted two series of experimental evaluations of pulsed blowing devices on the Circulation Control Wing (CCW) airfoil shown in Figure 3 above. The first test consisted of 157 runs in the GTRI Model Test Facility (MTF) on pulsed blown airfoil configurations. The blown CCW airfoil with 30° dual-radius flap was installed in the 30x43-inch test section of the MTF, as shown in Figure 23. Only the 12" center section of the 30-inch span 2-D CCW model was employed for the pulsed blowing, and this was separated by the large end plates shown.

Figure 23- Pulsed-Blowing Airfoil Setup in the GTRI Model Test Facility research tunnel, w/C=35%

These tests employed a set of solenoid valves external to the model to produce the pulsed blowing, but these were found to be relatively unresponsive at higher frequencies. Hot wire probes inserted in the blowing slots were used to map the velocity profiles of the jets during both pulsed and steady blowing, and showed these pulse devices to be relatively ineffective above about 15 cycles per second. Figure 24 shows these velocity measurements at the slot. It is seen that the average velocity and the peaks decay as the frequency increases. In no case is the desired square waveform achieved, where peak pressure is twice the average value and the minimum is zero. It was decided that this pulsing mechanism was inadequate.

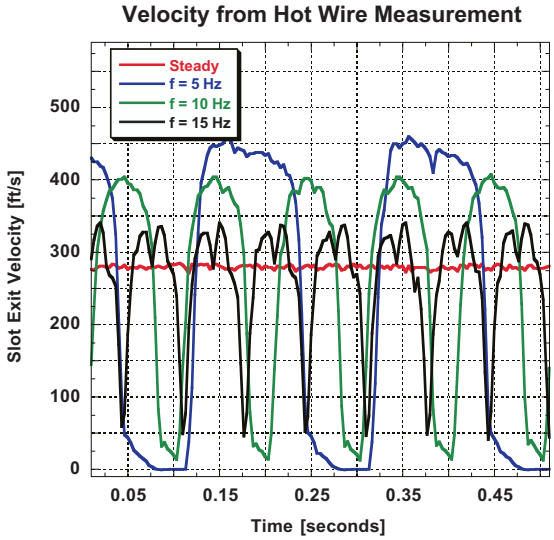

Figure 24- Measured blowing jet velocities at the slot compared to steady-state value at approximately 0.6 psig and average Cμ=0.035

Thus a second test series was conducted. This series employed torque motors with sliding shuttles and much higher frequency capability, and the pulsing range available was amplified by a factor of 4, now going to above 60Hz. These results showed that for a desired lift coefficient produced by the blown airfoil, the same C_L could be achieved by pulsing and using much less slot mass flow; see Figures 25. An increase in frequency shows an improvement in reducing mass flow requirements until the pulse train is distorted and attenuated. This optimum occurs at frequencies greater than 10 Hz, but is limited here by the performance of the actuator system. This is similar to the GACC results but now at a higher constant lift coefficient of 2.8-3.0. This in part is due to the streamline deflection created by the camber effects of the flap. The pulsed performance at these lift conditions is achieved with a 42-50% reduction in the required mass flow. It should be noted, of course, that with the same time-averaged mass flow, pulsed blowing generates considerably higher lift.

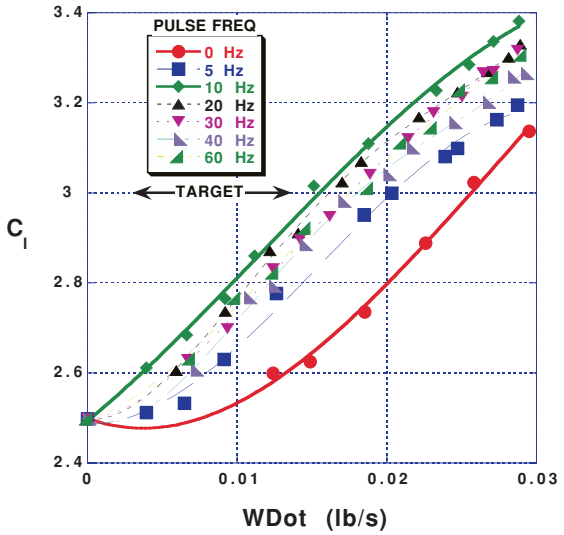

Figure 25 Comparison of pulsed and steady pneumatic control for the GTRI Dual-Radius CCW Airfoil with 30° flap deflection (Duty Cycle 50% and varying Frequency)

Note that for all of the above data, the averaged Cμ is determined from measured average mass flow (buffered flow-meter) multiplied by isentropic jet velocity that is calculated from the total pressure as measured by a high frequency unsteady dynamic pressure transducer installed in the plenum. Figure 26 compares the jet velocity measured by hot wire to that from the high frequency unsteady pressure transducer, both at a frequency of 15 Hz. Note that the averaged jet velocity from the unsteady pressure transducer appears to be considerably higher than the true values from the hot wire. Figure 27 compares unsteady results plotted as a function of unsteady Cμ. Thus, true average Cμ as calculated from the true time-averaged jet velocities will also be considerably lower than the actual values shown in Figure 27, and the true results of pulsed blowing indicated in Figure 28 could be much more than shown. Both Figures 27 and 28 show average C_L can be obtained with reduced mass flow or Cμ, but that higher frequencies begin to fade in benefits, at least from these device-limited experiments. Note however that in Figure 27, virtually all pulsed Cμ values tested exceed the steady-state curve in at least some range of blowing. Figure 28 further identifies the test problems associated with the generation of the desired square-wave form during, shown here at a frequency of 40Hz.

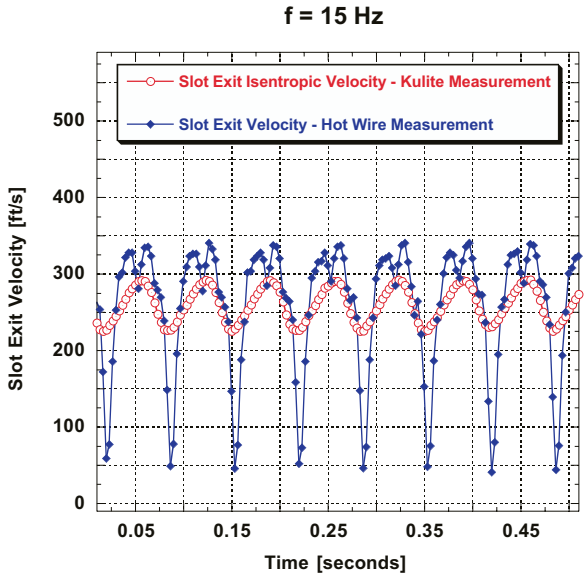

Figure 26- Measured Jet Velocity Compared to Velocities determined from Unsteady Plenum Total Pressure Measurements

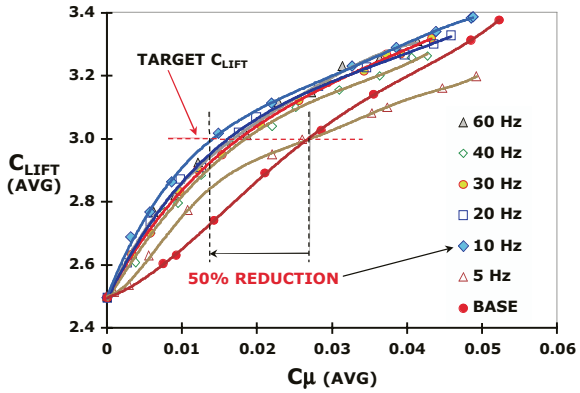

Figure 27- Comparison of Pulsed and Steady-state Lift as a function of Cμ, corresponding to Figure 22

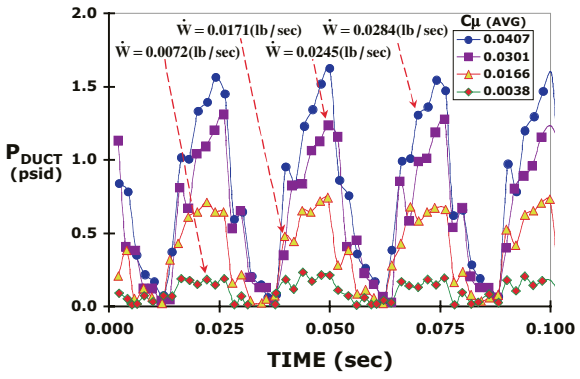

Figure 28- Pressure Wave Traces in the CCW Plenum at 40Hz with 4 Different Flow Rates and Cμ

CFD Analyses: It is recognized that time accurate (unsteady) circulation controlled airfoils provide several significant challenges for CFD technologies. Turbulence models and grid refinement compound the sensitivities of performance to boundary layer separation and jet interaction.[22] The ability to predict the performance of CC applications is therefore limited and CFD results will be used as a guide for understanding the salient features of the flow-field.

Because of the mechanical limits on the unsteady actuators, the above tests were limited to low frequencies. To gain a better understanding regarding the high frequency impact of pulsed CC, a preliminary analysis of frequencies as high as 400 Hz was performed using a time-dependant CFD RANS code described in References 23 And 24. The GTRI Dual Radius CCW airfoil configuration was modeled with the CCW flap deflected only 30°. In Figure 29, it appears that all pulsed curves are lower than the steady-state value, but this is because the mass flow rates required are different. Figure 30 plots the same lift data versus averaged mass flow, and labels points A through D for the same mass flow (0.00088 slug/sec). Now the higher frequencies produce greater ΔC_L than the steady state, or achieve the same ΔC_L at lower mass flow. While the lesser frequency curve eventually crosses over the steady-state curve, the 400Hz curve never does. Figure 31 shows further benefits of pulsed blowing by showing the equivalent efficiency (lift-to-drag ratio, L/D_{eq}) for these airfoils. Here, the blowing coefficient has been added to the drag coefficient (see Ref.25) to account for the blowing penalty. Note that the maximum can be achieved by the 400 Hz pulsed jet at roughly 32% lower mass flow required. At lower values of L/D_{eq} , mass flow required is less than 50% that for the steady-state case. It appears from these numerical predictions that there is further benefit to be gained by higher frequency pulsed blowing, and that experimental means should be devised to investigate these conditions.

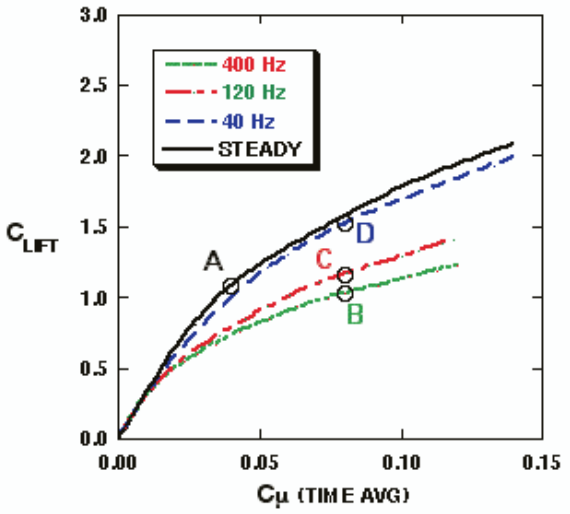

Figure 29- Time accurate CFD-Prediction of incremental Lift Coefficient for GTRI Airfoil, 30° CCW Flap

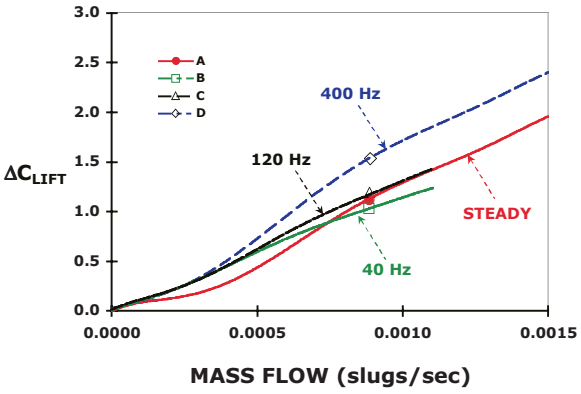

Figure 30- CFD-Predicted Incremental CL vs. Time-Averaged Mass Flow Rate

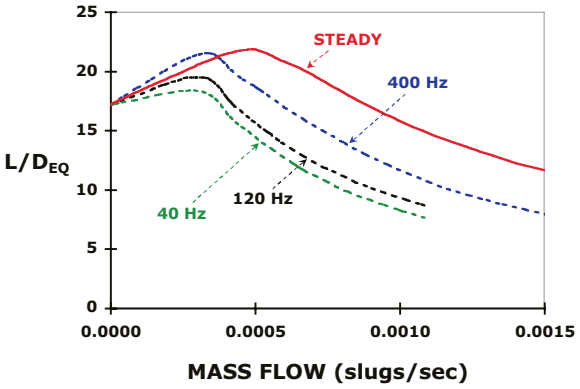

Figure 31- CFD-Predicted Airfoil Efficiency vs. Time-Averaged Mass Flow Rate

CONCLUDING REMARKS

Two independent experimental investigations have been conducted to evaluate the ability of pulsed blowing to reduce the mass flow requirements for high lift generation of CCW–type blown configurations. The basic difference in these CCW configurations is founded in the streamline turning mechanisms. The GACC required more jet entrainment to achieve the same streamline deflection as the Dual Radius CCW configuration. However the Dual Radius is limited in streamline turning by it's fixed separation defined by the tip of the flap (135°), whereas the GACC airfoil has a greater potential for larger streamline turning as jet separation extends onto the lower Coanda surface well beyond 165°. These limits were not evaluated in these experiments.

Pulsed pneumatic control for both the Dual-Radius and GACC airfoil configurations tested, reduced the mass flow requirements for a desired C_L by more than 50%. Conversely, for the same available mass flow rates, pulsing allowed considerably higher lift to be generated. Due to limitations in the pulsed actuator systems, the benefit of pulsed blowing was limited to separation control. It is believed that similar mass flow reductions can be achieved in the super-circulation region where time dependent penetration would occur.

These blown airfoil configurations also showed the ability to reduce cruise drag either by retraction of a small-chord curved CCW flap or by creating a "virtual" sharp trailing edge by blowing both the upper and lower slots of a dual-slot configuration. Pulsed blowing configurations also verified that they could achieve the same equivalent lift-to-drag ratio as the steady-state case, but at 55-60% reductions in required mass flow rates. CFD analyses presented indicated that additional gains could be expected from pulsed blowing at higher frequencies, but the experimental mechanisms of the current tests have not yet achieved that capability. Thus a goal of future research should be continuation of this development of pulsed blowing devices by improvements in higher-speed pulsing mechanisms.

REFERENCES

[1] Wilson, M.B., and Von Kerczek, C., "An Inventory of Some Force Producers for Use in Marine Vehicle Control," David Taylor Naval Ship R&D Center Report DTNSRDC-79/097, November 1979

[2] Wood, N.J., and Nielsen, J.N., "Circulation Control Airfoils Past, Present, Future," Paper AIAA 85-0204, AIAA 23rd Aerospace Sciences Meeting, Reno, Nevada, 1985

[3] Englar, R. J., "Circulation Control Pneumatic Aerodynamics: Blown Force and Moment Augmentation and Modification; Past, Present and Future," AIAA Paper 2000-2541, presented at AIAA Fluids 2000 Meeting, Denver, CO, June 19-22, 2000.

[4] Englar, R. J. and Applegate, C.A., "Circulation Control--A Bibliography of DTNTSRC Research and Selected Outside References (January 1969 through December 1983), DTRNRDC-84/052, Sept 1984

[5] Imber, R.D., and Rogers, E.O., "Investigation of a Circular Planform Wing with Tangential Fluid Ejection," AIAA, January 1996

[6] Abramson, J., and Rogers, E.O., "High-Speed Characteristics of Circulation Control Airfoils," AIAA-83-0265, January 1983

[7] Rogers, E.O., "Development of Compressible Flow Similarity Concepts for Circulation Control Airfoils," AIAA-87-0153, January 1987

[8] Englar, R.J., and Williams, R.M., "Design of Circulation Controlled Stern Plane for Submarine Applications," David Taylor Naval Ship R&D Center Report NSRDC/AL-200 (AD901-198), March 1971

[9] Sellers, W.L., Jones, G.S., and Moore, M.D., "Flow Control Research at NASA Langley in Support of High-Lift Augmentation," AIAA-2002-6006

[10] Cagle, C.M. and Jones, G.S., "A Wind Tunnel Model to Explore Unsteady Circulation Control for General Aviation Applications," AIAA paper 2002-3240, June 2002.

[11] Jones, G.S., Viken, S.A., Washburn, A/E., Jenkins, L.N., and Cagle, C.M., "An Active Flow Circulation Controlled Flap Concept for General Aviation Aircraft Applications, "AIAA Paper 2002-3157, June, 2002.

[12] Englar, R. J., Smith, M. J., Kelley, S. M., and Rover, R. C. III, "Application of Circulation Control Technology to Advanced Subsonic Transport Aircraft, Part I: Airfoil Development," AIAA Paper No. 93-0644, AIAA *Journal of Aircraft,* Vol. 31, No. 5, pp. 1160-1168, Sept-Oct. 1994.

[13] Metral, A.R., "On the Phenomenon of Fluid Veins and Their Applications, the Coanda Effect," AF Translation, F-TS-786-RE, 1939

[14] Schlichtling, H., Boundary layer Theory, 2nd edition, pp. 750-751, 1979

[15] Kizilos, A.P., "Fluid Flight Control Feasibility Study using the Variable Deflection Thruster," Honeywell AD: 378303, December 9, 1966

[16] Sellers, W.L., III and Kjelgaard, S. O.: The Basic Aerodynamics Research Tunnel - A Facility Dedicated to Code Validation, AIAA-88-1997, May 1988.

[17] Hall, D. W., "Personal Air Vehicle Exploration (PAVE)," PAVE workshop, Jan. 8, 2002

[18] Kind, R.J., and Maull, D.J., "An Experimental Investigation of a Low-Speed Circulation-Controlled Aerofoil," The Aeronautical Quarterly, July 1967

[19] Oyler, T.E. and Palmer, W. E., "Exploratory Investigations of Pulse Blowing for Boundary layer Control," Columbus Division, North American Rockwell Corp, Report NR72H-12

[20] Walters, R.E., Myer, D.P., and Holt, D.J., "Circulation Control by Steady and Pulsed Blowing for a Cambered Elliptical Airfoil," West Virginia University TR-32, July 1972

[21] Schaeffler, N.M., Hepner, T.E., Jones, G.S. and Kegerise, M.A., "Overview of Active Flow Control Actuator Development at NASA Langley Research Center," AIAA Paper 2002-3159, June 2002

[22] Slomski, J, and Marino, T., "Navy Successfully Simulates Effect that may Improve Low-Speed Maneuverability," Ocean News and Technology, November 2002

[23] Liu, Y., Sankar, L., Englar, R., and Ahuja, K., "Numerical Simulation of the Steady and Unsteady Aerodynamic Characteristics of a Circulation Control Wing," AIAA Paper 2001-0704, AIAA 39th Aerospace Sciences Meeting, Reno, NV, January 8-11, 2001

[24] Liu, Y., "Numerical Simulations of the Aerodynamic Characteristics of Circulation Control Wing Sections", PhD Thesis, Georgia Institute of Technology, March, 2003.

[25] Englar, R. J. and Williams, R.M., "Test Techniques for High Lift Two- Dimensional Airfoils with Boundary Layer and Circulation Control for Application to Rotary Wing Aircraft," *Canadian Aeronautics and Space Journal*, Vol. 19, No. 3, pp. 93-108,Mar 1973.